# Stem cell-released oncolytic herpes simplex virus has therapeutic efficacy in brain metastatic melanomas

Wanlu Du[a], Ivan Seah[a], Oumaima Bougazzoul[a], GiHun Choi[a,b], Katrina Meeth[c], Marcus W. Bosenberg[c,d], Hiroaki Wakimoto[a,b,e], David Fisher[f], and Khalid Shah[a,b,g,h,1]

[a]Center for Stem Cell Therapeutics and Imaging, Department of Radiology, Massachusetts General Hospital, Harvard Medical School, Boston, MA 02114; [b]Center for Stem Cell Therapeutics and Imaging Department of Neurosurgery, Brigham and Women's Hospital, Harvard Medical School, Boston, MA 02115; [c]Department of Pathology, Yale School of Medicine, New Haven, CT 06520; [d]Department of Dermatology, Yale School of Medicine, New Haven, CT 06520; [e]Department of Neurosurgery, Massachusetts General Hospital, Harvard Medical School, Boston, MA 02114; [f]Department of Dermatology, Massachusetts General Hospital, Harvard Medical School, Boston, MA 02114; [g]Department of Neurology, Massachusetts General Hospital, Harvard Medical School, Boston, MA 02114; and [h]Harvard Stem Cell Institute, Harvard University, Cambridge, MA 02138

Edited by Patrick S. Moore, University of Pittsburgh Cancer Institute, Pittsburgh, PA, and approved June 8, 2017 (received for review January 8, 2017)

**The recent Food and Drug Administration approval of immunogenic oncolytic virus (OV) has opened a new era in the treatment of advanced melanoma; however, approximately 50% of patients with melanoma develop brain metastasis, and currently there are no beneficial treatment options for such patients. To model the progression of metastases seen in patients and to overcome the hurdles of systemic delivery of OV, we developed melanoma brain metastasis models in immunocompromised and immunocompetent mice, and tested the fate and efficacy of oncolytic herpes simplex virus (oHSV)-armed mesenchymal stem cells (MSCs). Using brain-seeking patient-derived melanoma cells and real-time in vivo imaging, we show a widespread distribution of micrometastases and macrometastases in the brain, recapitulating the progression of multifoci metastases seen in patients. We armed MSCs with different oHSV variants (MSC-oHSV) and found that intracarotid administration of MSC-oHSV, but not of purified oHSV alone, effectively tracks metastatic tumor lesions and significantly prolongs the survival of brain tumor-bearing mice. In a syngeneic model of melanoma brain metastasis, a combination of MSC-oHSV and PD-L1 blockade increases IFNγ-producing $CD8^+$ tumor-infiltrating T lymphocytes and results in a profound extension of the median survival of treated animals. This study thus demonstrates the utility of MSCs as OV carriers to disseminated brain lesions, and provides a clinically applicable therapeutic platform to target melanoma brain metastasis.**

stem cells | oncolytic virus | tumors | metastasis | imaging

Melanoma, the most aggressive type of skin cancer, accounts for a large proportion of skin cancer-related deaths (1). Among all cancer types, melanoma has a particularly high propensity to metastasize to the brain, occurring in >50% of all patients with advanced disease. More than 90% of melanoma brain metastases lead to death, and the median survival is 17–22 wk after detection (2–4).

Current therapeutic options of chemotherapy, surgery, and radiation have very limited efficacy for patients with melanoma brain metastasis (5–7). These patients either have multiple metastatic lesions or diagnostically challenging asymptomatic lesions, making surgery an inadequate therapeutic option by itself. In addition, the blood-brain barrier (BBB) limits central nervous system (CNS) penetration of systemic therapies, and the negative side effects of radiotherapy (8) pose challenges for the success of existing therapies, contributing to the failure to improve overall patient survival. As such, there is an urgent need for new therapies for melanoma brain metastasis.

The development and characterization of preclinical tumor models that authentically recapitulate the clinical disease settings are critical for developing and testing new therapies. Most previous studies have used either subcutaneous (s.c.) injection or intracranial injection of established melanoma lines in mice (9–11), which do not mimic the actual clinical settings of melanoma brain metastasis, such as initial adhesion of tumor cells to brain capillaries, extravasation, continuation of perivascular position, vessel co-option, micrometastatic growth, and macrometastatic growth (12). In addition, long-established melanoma lines often fail to recapitulate the key aspects of human malignancy and thus poorly predict the clinical efficacy of tested therapeutic agents (13).

In this study, we created in vivo imageable mouse models of melanoma brain metastasis by internal carotid artery (ICA) injection of patient-derived primary melanoma and brain-seeking melanoma lines [either *BRAF* mutant or wild type (WT)], as well as the syngeneic mouse model of melanoma brain metastasis using a *BRAF* mutant line isolated from $Braf^{V600E/wt}Cdkn2A^{-/-}Pten^{-/-}$ mice.

Oncolytic viruses (OVs) that selectively replicate in tumor cells are an emerging modality of cancer treatment that shows promising results in both preclinical studies and clinical trials (14, 15). Among these OVs, oncolytic herpes simplex viruses (oHSV) have shown promising therapeutic efficacy in treating advanced melanoma (16, 17). Recently, the US Food and Drug Administration approved talimogene laherparepvec (T-VEC) for the treatment of melanoma lesions in the skin and lymph nodes (17). Although induction of an antitumor immune response is implicated in activity for distant uninjected lesions, T-VEC has not been shown to improve overall patient survival of stage IVM1b and IVM1c disease that has metastatic lesions to the brain, bone, liver, lungs, or other internal organs (18). The unavailability of appropriate clinically translatable mouse models of melanoma brain metastasis and issues related to oHSV delivery via the bloodstream (19), such as virus neutralization, sequestration, and inefficient extravasation, pose major barriers to the development of oHSV-based therapies for melanoma brain metastasis.

## Significance

**This study provides an insight into stem cell-based oncolytic virus therapies for advanced melanoma tumors that have metastasized into the brain by developing clinically relevant mouse tumor models and testing the fate and efficacy of oncolytic herpes simplex virus-armed mesenchymal stem cells in such models. This study therefore overcomes the hurdles of systemic delivery of oncolytic viruses and provides a clinically applicable therapeutic platform to target melanoma brain metastasis.**

Author contributions: W.D. and K.S. designed research; W.D., I.S., O.B., G.C., and H.W. performed research; W.D., K.M., M.W.B., H.W., and D.F. contributed new reagents/analytic tools; W.D., I.S., O.B., G.C., H.W., D.F., and K.S. analyzed data; and W.D., H.W., D.F., and K.S. wrote the paper.

Conflict of interest statement: K.S. owns equity in, and is a member of the Board of Directors of, AMASA Technologies.

This article is a PNAS Direct Submission.

[1]To whom correspondence should be addressed. Email: kshah@bwh.harvard.edu.

This article contains supporting information online at www.pnas.org/lookup/suppl/doi:10.1073/pnas.1700363114/-/DCSupplemental.

Previous studies from our laboratory demonstrated that therapeutic human and mouse stem cells home extensively to multiple tumor deposits in the brain (20) and act as cell carriers for onsite delivery of tumor-specific agents or OV (21) in mouse models of different brain tumor types (22). In the present study, we tested the therapeutic efficacy of MSC-loaded oHSV (MSC-oHSV) in both *BRAF* mutant and WT in vivo imageable mouse models of melanoma brain metastasis, and explored the combined therapeutic efficacy of PD-L1 blockade and MSC-oHSV in a syngeneic mouse model of melanoma brain metastasis.

## Results

**A Panel of Human Melanoma Lines Respond to oHSV.** Considering both malignancy and mutational status (23), we chose both established malignant human melanoma lines (SK-Mel-2, SK-Mel-28, MALME-3M, and MeWo) and patient-derived brain metastatic melanoma lines (TXM-13, M12, and M15). We tested the efficacy of the G47Δ-based recombinant oHSV in which cDNA encoding the mCherry fluorescent protein is placed under the IE4/5 immediate-early promoter of HSV (oHSV-mCh) on these lines. Low-multiplicity of infection (MOI) oHSV-mCh infection led to rapid production and spread of oHSV in tumor cells over time (Fig. 1 *A* and *B*), which resulted in robust dose-dependent cell killing (Fig. 1*C*) in all tested cell lines but had no significant effect on the viability of normal nonproliferating human astrocyte cultures (*SI Appendix*, Fig. S1). In parallel, we tested the efficacy of promising clinically approved therapeutic agents for advanced melanoma patients. Cell viability assays revealed minor effects of BRAF inhibitor PLX4720 in *BRAF* mutant (SK-Mel-28, MALME-3M, and M12) melanoma lines and no effects in *BRAF* WT (SK-Mel-2, MeWo, TXM-13, and M15) lines (*SI Appendix*, Fig. S2*A*). Similarly, treatment with temozolomide (TMZ) and low-dose cisplatin showed marginal effects on melanoma cell viability (*SI Appendix*, Fig. S2 *B* and *C*). These results indicate the unique ability of oHSV to target a broad spectrum of malignant melanoma lines with a robust cell-killing effect regardless of their *BRAF* mutational status.

**Development and Characterization of Melanoma Brain Metastasis Mouse Models.** To establish in vivo melanoma brain metastasis mouse models that recapitulate the steps of metastatic progression seen in patients, we chose two human melanoma lines, MeWo (*BRAF* WT, pigmented), which was isolated from lymph nodes of a patient with advanced melanoma, and M12 (*BRAF* mutant, nonpigmented), which was directly isolated from a melanoma brain metastasis. Both cell lines were engineered to express a bimodal firefly luciferase (Fluc)-mCherry (FmC) protein (*SI Appendix*, Fig. S3 *A* and *B*). To mimic the critical steps of metastatic

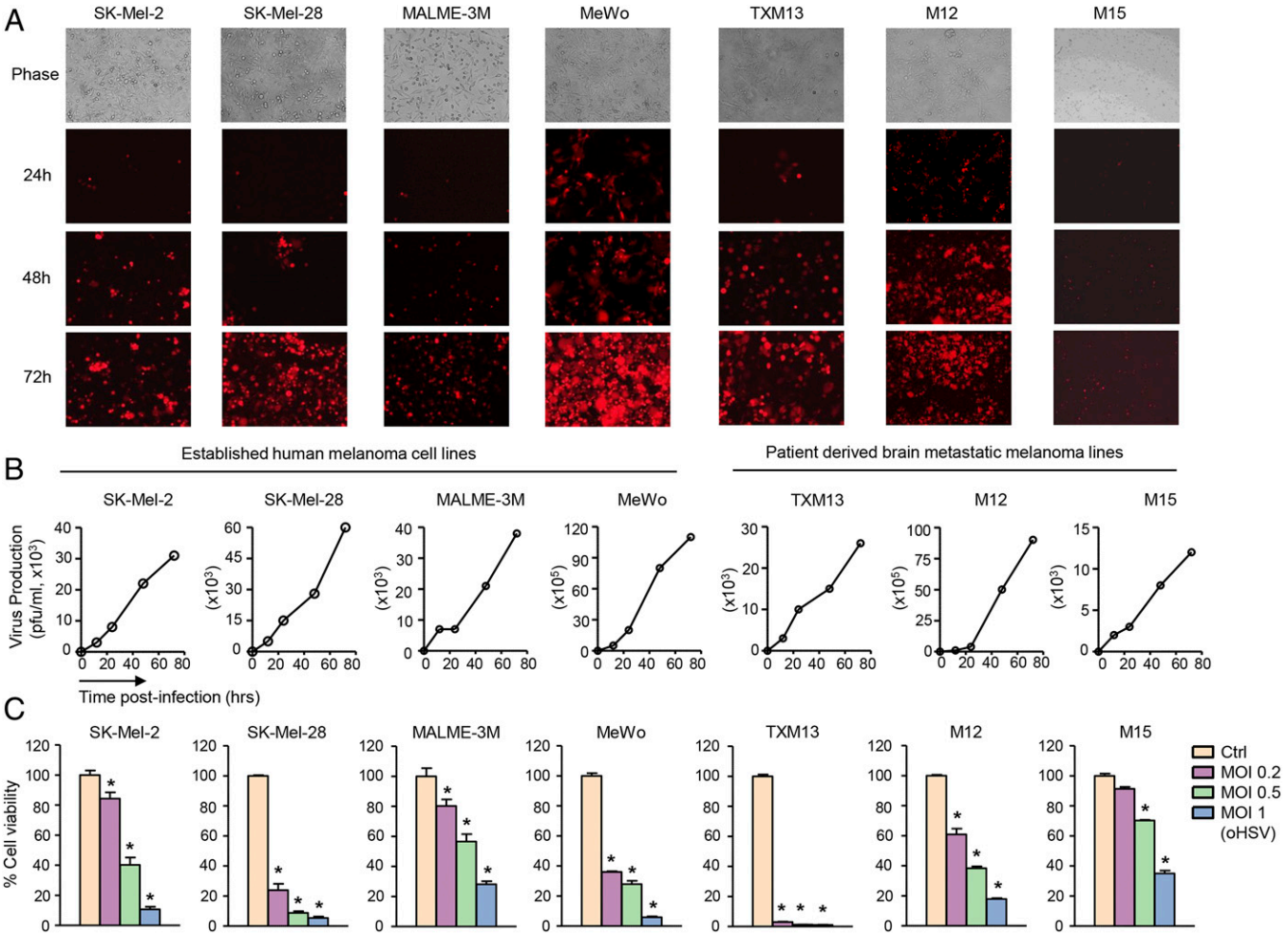


**Fig. 1.** oHSV replicates in human melanoma cells and kills them by viral oncolysis. (*A*) Four established human melanoma cell lines and three patient-derived brain metastatic melanoma cell lines were infected with oHSV-mCh at MOI of 0.2. Representative fluorescence microscopic images at different time points are shown. (Magnification: 10×) (*B*) Human melanoma cells were infected with oHSV, and the virus production postinfection was measured by a plaque assay. (*C*) Human melanoma cells were infected with oHSV at different MOI (0.2–1), and cell viability was analyzed at day 4 after virus infection. *$P < 0.05$ vs. uninfected controls (Ctrl).

colonization and blood vessel interactions, MeWo-FmC and M12-FmC were injected via the ICA into immunocompromised mice (Fig. 2*A*). Noninvasive bioluminescence imaging (BLI) of tumor-bearing mice revealed brain metastasis and exponential growth of metastatic tumors in the brain at 2–3 wk post-ICA injection of tumor cells (Fig. 2 *B* and *C*). Pigmented metastatic foci were seen in the brains bearing MeWo-FmC tumors (Fig. 2*D*), whereas no pathological changes were apparent in the brains bearing M12-FmC tumors (Fig. 2*H*). However, at a cellular level, fluorescent images confirmed the presence of mCherry-positive ($mCh^+$) tumor cells within macrometastatic foci in both models (Fig. 2 *E* and *I*).

Further immunohistochemistry analysis of brain sections from tumor-bearing mice demonstrated that metastatic melanoma cells ($mCh^+$) were proliferative ($Ki67^+$) and associated with reactive astrocytes ($GFAP^+$) (MeWo-FmC, Fig. 2 *F* and *G*; M12-FmC, Fig. 2 *J* and *K*). Coronal brain sections from mice bearing M12-FmC brain metastases at different time points after tumor cell injection showed that tumor cells distributed across all representative sections and the number and size of metastases increased over time, consistent with increased bioluminescence (Fig. 2*L*). Quantitative assessment of mCherry fluorescence on brain sections along the anteroposterior axis at 14, 21, and 28 d post–M12-FmC cell implantation revealed distinct tumor foci that were detectable as early as 14 d, along with widespread distribution of micrometastases and macrometastases in the later stages of metastatic progression (days 21 and 28; Fig. 2*M*). Our results show that ICA injection of patient-derived malignant melanoma cells generates clinically relevant mouse models that resemble the development of multifoci melanoma brain metastases observed in the clinic.

**MSCs Act as Cellular Vehicles for oHSV Delivery.** To assess the survival and viral spread of human MSCs freshly loaded with oHSV-mCh (MSC-oHSV-mCh) in vitro, MSCs were infected with oHSV-mCh at different MOI. The increased expression of mCherry within MSCs over time indicated efficient spread and amplification of oHSV-mCh (*SI Appendix*, Fig. S4). Cell viability assays of MSCs loaded with oHSV at different MOI showed that ∼90% of MSC-oHSV survived at least 4 d postinfection with an MOI of 0.2 or 0.5, and >60% MSC-oHSV survived with an MOI of 1 (Fig. 3*A*).

In parallel, we tested whether human MSCs had any influence on the growth of melanoma cells in culture and in vivo. We first engineered MeWo cells to express GFP (MeWo-GFP) and combined GFP and Fluc markers (MeWo-GFP-Fluc). Fluc bioluminescent imaging revealed that MSC cocultured with MeWo-GFP-Fluc cells or ICA-injected into mice bearing MeWo-GFP-Fluc tumors did not result in any changes in tumor cell growth in vitro or in vivo (*SI Appendix*, Fig. S5).

To further assess the oncolytic activity of MSC-released oHSV-mCh on melanoma cells, we cocultured MeWo-GFP cells with MSC-oHSV-mCh. Dual fluorescent imaging revealed the release of oHSV-mCh from MSCs (representative as red cell population), which resulted in the infection of adjacent MeWo-GFP cells and spread of oHSV-mCh among melanoma cells

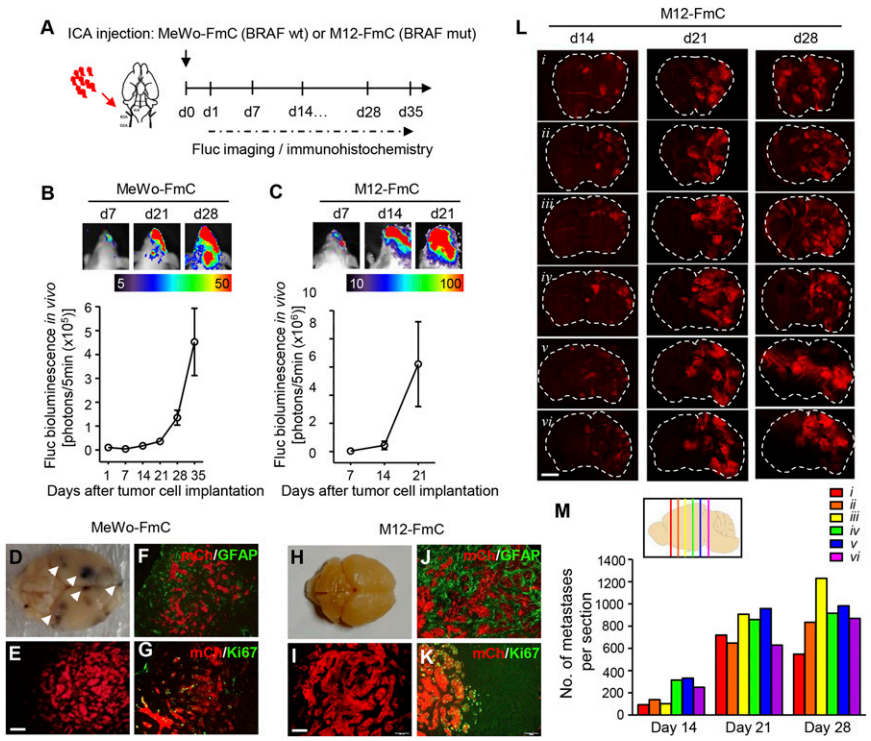


**Fig. 2.** Characterizing in vivo imageable melanoma brain metastasis mouse models. (*A*) Experimental outline showing tumor cell implantation and subsequent imaging/immunohistochemistry studies. Red arrow indicates the route of tumor cell injection. Black arrow indicates the time point of tumor cell implantation. (*B* and *C*) Representative bioluminescent images of MeWo-FmC (*B*) and M12-FmC (*C*) tumors after ICA injection of tumor cells (*Top*) and plot showing the in vivo tumor growth of MeWo-FmC or M12-FmC over time (*Bottom*); $n = 3$ mice per cell line. (*D* and *H*) Representative images showing multiple pigmented foci (white arrowheads) of MeWo-FmC ICA-injected mouse brain (*D*) and nonpigmented M12-FmC ICA-injected mouse brain (*H*). (*E* and *I*) Fluorescent images of metastatic foci in the brain: (*E*) MeWo-FmC; (*I*) M12-FmC. (*F*, *G*, *J*, and *K*) Representative fluorescent images of GFAP or Ki67 immunostaining (green) on brain sections showing proliferative metastatic melanoma cells ($Ki67^+$; $mCh^+$) surrounded by reactive astrocytes ($GFAP^+$). (*L*) Composite fluorescent images of coronal brain sections of mice bearing metastatic M12-FmC tumors from different planes along the anteroposterior axis (*i*–*vi*). (*M*) Quantification of micrometastatic and macrometastatic foci in the brain. (*Inset*) The location of each coronal section along the anteroposterior axis (*i*–*vi*). (Scale bars: *E* and *I*, 100 μm, also applies to *F*, *G*, *J*, and *K*; *L*, 2 mm.)

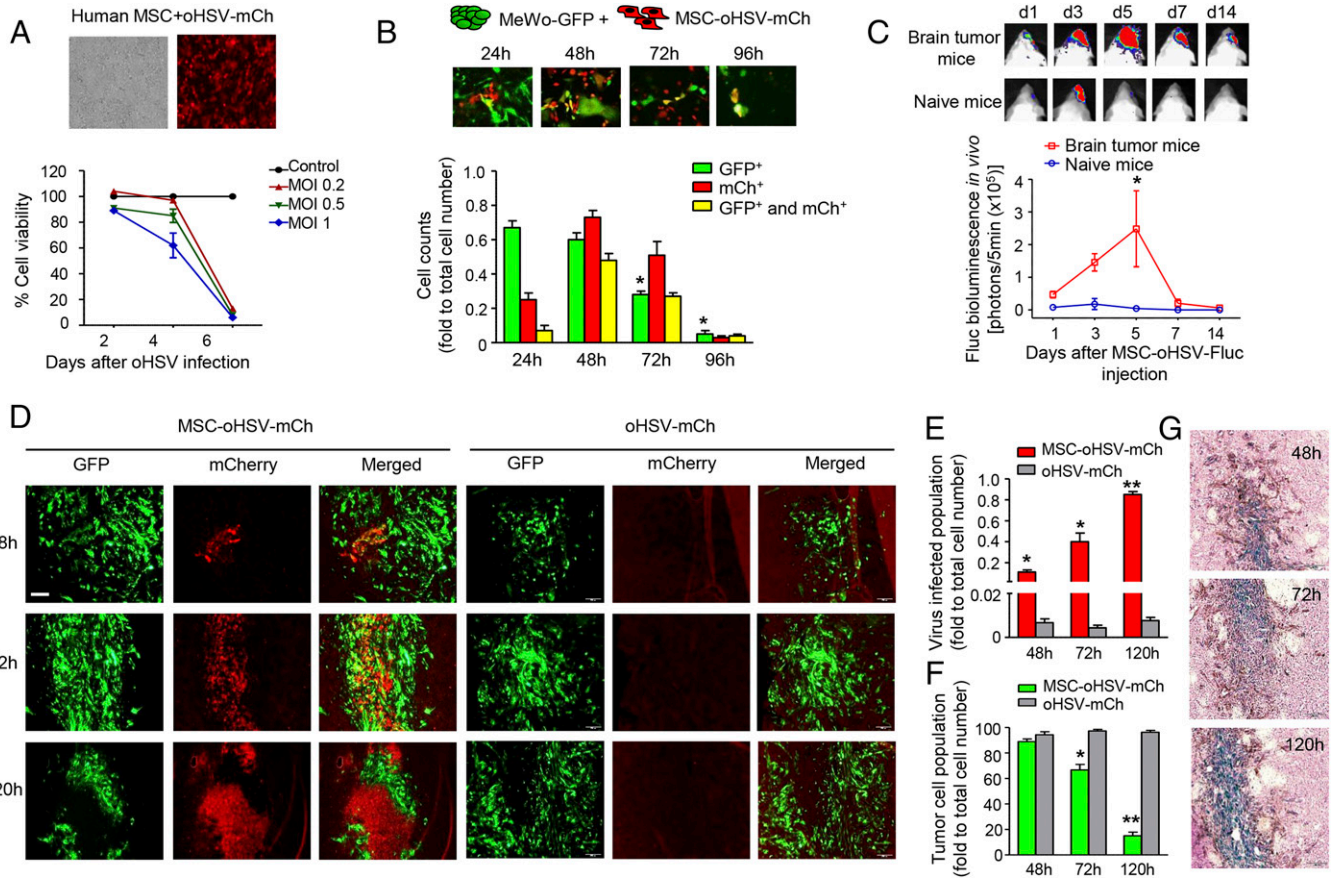


**Fig. 3.** In vivo imaging of MSC-mediated delivery of oHSV in mouse models of melanoma brain metastasis. (*A*) Cell viability of MSCs infected with oHSV-mCh at the indicated MOI analyzed at days 2, 4, and 6 postinfection. Representative phase and fluorescent images of human MSCs infected with oHSV-mCh at an MOI of 1 (24 h postinfection) are shown. (Magnification: 10×.) (*B*) MSC-oHSV-mCh were cocultured with MeWo-GFP at a 1:1 ratio, and populations of tumor cells (green), oHSV-mCh loaded MSCs (red), and oHSV-mCh–infected tumor cells (yellow) were analyzed at different time points. Representative fluorescent images show the coculture of MeWo-GFP and MSC-oHSV-mCh over time. (Magnification: 20×.) (*C*) Plot showing Fluc activity after MSC-oHSV-Fluc ICA injection in the melanoma metastatic brain tumor mice group and naive mice group. Representative bioluminescent images at different time points are shown. $*P < 0.05$ vs. naive mice ($n = 3$ mice per group). (*D*) Fluorescent images showing the population of tumor cells ($GFP^+$) and oHSV-mCh–infected cells ($mCh^+$) after ICA injection of MSC-oHSV-mCh or purified oHSV-mCh at the indicated time points. (Scale bar: 100 μm.) (*E* and *F*) Plots showing the populations of oHSV-mCh–infected cells (*E*) and tumor cells only (*F*) in the brain at different time points after ICA injection of MSC-oHSV-mCh or purified oHSV-mCh. $*P < 0.05$, $**P < 0.01$ vs. the oHSV-mCh–injected group ($n = 3$ mice per group). (*G*) Photomicrographs showing the time-dependent increase in $LacZ^+$-infected cells after ICA injection of MSC-oHSV-mCh. (Magnification: 10×.)

(representative as yellow cell population), leading to extensive oncolysis and a significant decrease in tumor cell number (green cell population) (Fig. 3*B*).

To visualize the activity and dynamics of oHSV delivered by MSCs in vivo, we used an oHSV bearing Fluc (oHSV-Fluc). MSCs freshly infected with oHSV-Fluc (MSC-oHSV-Fluc) were injected either via the ICA or i.v. into brain tumor-bearing mice and naive mice (non–tumor-bearing). An in vivo Fluc BLI signal indicating viral infection was detected as early as day 1 after MSC-oHSV-Fluc injection via the ICA, with a significant increase at day 5 in the brain tumor-bearing mice compared with the naive mice (Fig. 3*C*). The Fluc signals were detected exclusively in the brains of tumor-bearing mice, indicating that the majority of MSC-oHSV-Fluc cells home to tumor lesions in the brain upon ICA administration (*SI Appendix*, Fig. S6*A*). However, no Fluc BLI signal intensity was seen in the brain when MSC-oHSV-Fluc cells were injected i.v. into mice bearing MeWo-Rluc tumors. Instead, significant Fluc BLI intensity was seen in the lung, indicating that the vast majority of i.v.-injected cells were trapped in the lung (*SI Appendix*, Fig. S6*B*).

To further confirm the presence of oHSV within brain tumor lesions at cellular resolution after ICA injection, mice bearing MeWo-GFP tumors were ICA-injected with MSC-oHSV-mCh. Multicolor fluorescence imaging of serial brain sections from mice killed at different time points showed a rapid spread of oHSV-mCh emanating from a small population of MSC-oHSV-mCh cells within tumor deposits in the brain, with concomitant shrinkage of MeWo-GFP tumor areas within 120 h (Fig. 3*D*). In contrast, ICA injection of purified oHSV-mCh did not result in detectable mCherry fluorescence in melanoma-bearing mice, with no effects on $GFP^+$ tumor areas (Fig. 3*D*). Quantification of the fluorescent imaging results revealed a continuous increase in the oHSV-mCh-infected cell population in the brains of tumor-bearing mice with ICA-injected MSC-oHSV-mCh (Fig. 3*E*) and a concurrent decrease in the $GFP^+$ tumor cell population (Fig. 3*F*), a stark contrast to the observations with purified oHSV-mCh administration via the ICA.

X-gal staining on brain sections from mice bearing tumors injected with MSC-oHSV-mCh via the ICA revealed a time-dependent increase specifically in the oHSV reporter lacZ-positive pigmented tumors cells (Fig. 3*G*). Similar homing of MSC-oHSV-mCh was observed in mice bearing M12-GFP-Fluc tumor deposits in the brain (*SI Appendix*, Fig. S7). These data further confirm the transfer of oHSV from MSCs to tumor cells and the subsequent

infection of tumor cells while leaving the normal brain cells behind. These results show that intra-arterially administrated MSC-oHSV, but not purified oHSV, track and eliminate melanoma tumor cells in the brain.

**MSC-oHSV has Therapeutic Efficacy in Both BRAF WT and Mutant Mouse Models of Melanoma Brain Metastasis.** We next sought to determine the therapeutic potential of MSC-oHSV in mouse models of melanoma brain metastasis (Fig. 4*A*). BLI imaging revealed a significant remission of metastatic tumor burden in the brains of MeWo-FmC-bearing mice treated with MSC-oHSV compared with continuous tumor growth by treatment with uninfected MSCs (Fig. 4 *B* and *C*). This was further confirmed by a significant decrease in the number of pigmented lesions in the brains of the MSC-oHSV–treated group compared with controls (Fig. 4*D*), resulting in a significant survival benefit in treated mice (Fig. 4*E*). Similar studies were performed in mice bearing M12-FmC tumors. Treatment with MSC-oHSV significantly inhibited metastatic tumor growth in the brains of M12-FmC–bearing mice compared with controls (Fig. 4 *F* and *G*). This was further confirmed by a significant decrease in the number of Ki67$^{+}$ proliferative tumor cells in the brain lesions of the MSC-oHSV–treated group compared with controls (Fig. 4*H*), resulting in prolonged survival

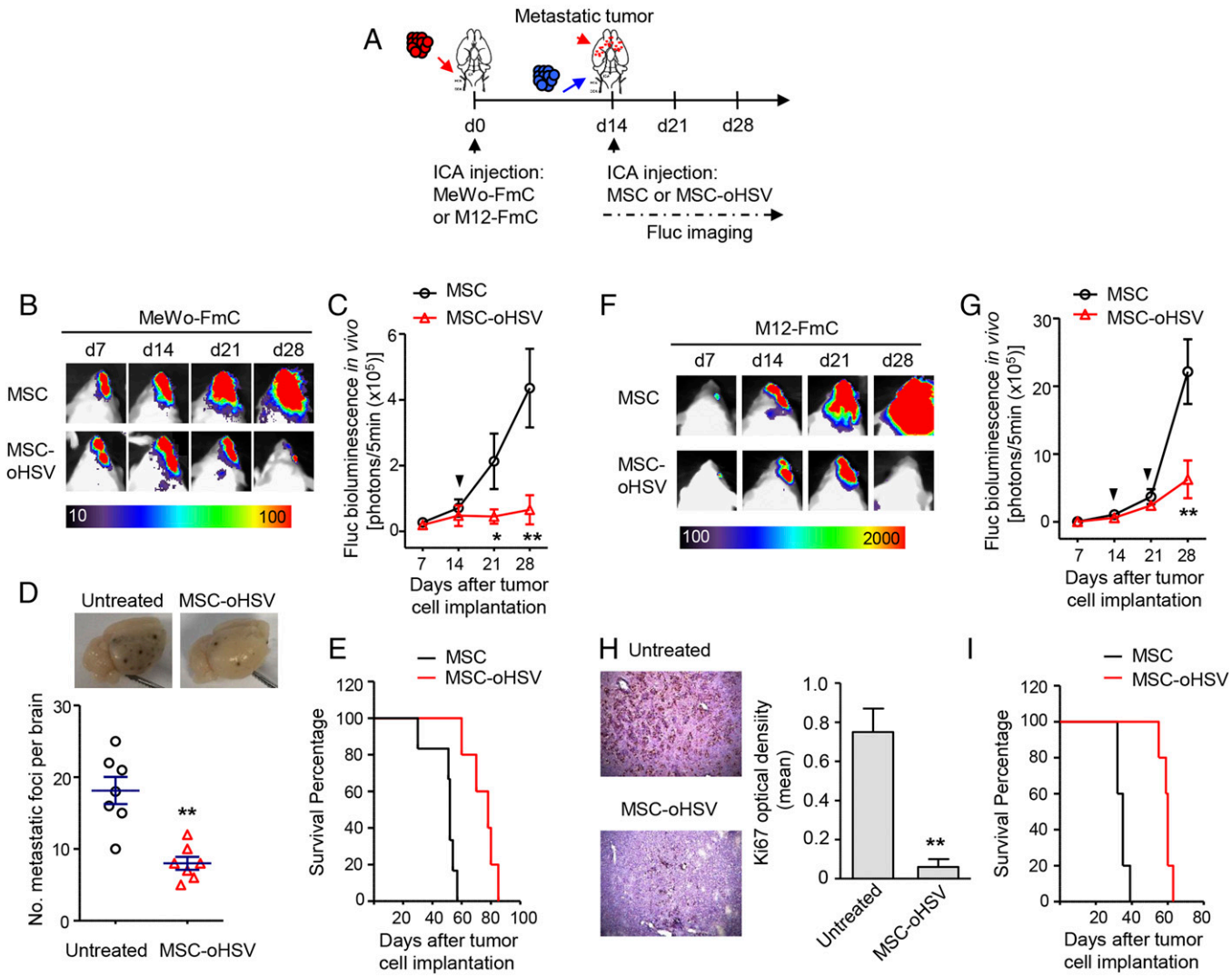


**Fig. 4.** ICA-delivered MSC-oHSV have therapeutic efficacy in melanoma brain metastasis derived from human BRAF WT and mutant melanoma lines. (*A*) Experimental outline. Red arrow indicates the route of tumor cell injection. Red arrowhead indicates the multiple tumor deposits in the brain. Blue arrow indicates the route for stem cell administration. (*B*) Representative bioluminescence images of MeWo-FmC–tumor bearing mice treated with MSC-oHSV or MSCs. (*C*) Plot of bioluminescence signal changes showing in vivo MeWo-FmC tumor growth after MSC-oHSV treatment. $*P < 0.05$, $**P < 0.01$ vs. the MSC-treated group ($n = 5$ mice per group). The black arrowhead indicates the time point of MSC or MSC-oHSV administration. (*D*) Representative images of pigmented metastatic foci in the brains of MSC-oHSV–treated and untreated mice at 4 wk after tumor cell implantation. $**P < 0.01$ vs. untreated control group ($n = 7$ mice per group). (*E*) Kaplan–Meier survival curves of MeWo-FmC tumor-bearing mice treated with MSC-oHSV or control MSCs. $P = 0.0014$ in the MSC-oHSV and control MSC comparison, log-rank test ($n = 6$ mice per group). (*F*) Representative bioluminescence images of M12-FmC tumor-bearing mice treated with MSC-oHSV or control MSCs. (*G*) Plot of bioluminescence signal changes showing in vivo M12-FmC tumor growth in MSC-oHSV– and control MSC-treated groups. $**P < 0.01$ vs. MSC-treated group ($n = 5$ mice per group). Black arrowheads indicate the two time points for MSC or MSC-oHSV administration. The second treatment was delivered via the contralateral ICA. (*H*) Immunohistochemistry-DAB images of Ki67 on brain sections and plot showing the optical density of Ki67 staining from MSC-oHSV–treated and untreated mice at 4 wk after tumor cell implantation. $**P < 0.01$ vs. untreated control group ($n = 3$ mice per group). (Magnification: 10×.) (*I*) Kaplan–Meier survival curves of M12-FmC tumor-bearing mice treated with MSC-oHSV or control MSCs. $P = 0.0019$ in the MSC-oHSV and control MSC comparison, log-rank test ($n = 5$ mice per group).

of MSC-oHSV–treated mice bearing M12-FmC brain tumors (Fig. 4*I*). These results demonstrate that intra-arterially administrated MSCs serve as robust cellular vehicles for delivering therapeutic oHSV to target and eliminate multiple metastatic deposits in the brain.

**Characterization of the Syngeneic Melanoma Brain Metastasis Mouse Model.** Although direct antitumor properties were originally considered the main mechanism of OVs, an increasing body of evidence suggests that the host immune response may be critical to the efficacy of oncolytic virotherapy (24). This may be mediated via innate immune effectors or via antiviral or antitumor adaptive cellular immune responses. Therefore, the use of an immunocompetent melanoma model to study the efficacy of MSC-oHSV is critical. We hypothesized that MSC-oHSV will synergize with immune checkpoint blockers, such as those that target the PD-1/PD-L1 pathway. To investigate the therapeutic efficacy of MSC-oHSV in combination with anti–PD-L1 immunotherapy, we successfully developed a syngeneic mouse model of melanoma brain metastasis by ICA injection of YUMM1.1 cells derived from an induced tumor in congenic C57BL/6 Tyr::CreER/Braf$^{V600E}$/$^{wt}$Cdkn2A$^{-/-}$Pten$^{-/-}$ mice. The YUMM1.1 cells were engineered to express GFP-Fluc (Y1.1-GFl; *SI Appendix*, Fig. S8*A*) and were ICA-injected in immunocompetent C57BL/6 mice. BLI on tumor-bearing mice revealed exclusive tumor growth in the brain (*SI Appendix*, Fig. S8 *B* and *C*) and the exponential growth of metastatic tumor in the brain at 3 wk after Y1.1-GFl implantation (Fig. 5 *A* and *B*), eventually resulting in mouse mortality. In vitro immunocytochemistry analysis showed that YUMM1.1 cells express both S100β, the melanoma biomarker protein, and PD-L1 (*SI Appendix*, Fig. S9*A*). In vivo, H&E staining showed the presence of multiple metastatic foci in mice brains (Fig. 5 *C*–*E*). Immunohistochemical analysis of brain sections from melanoma brain metastasis revealed an association of reactive astrocytes (GFAP$^+$) with metastatic tumor cells, suggesting an inflammatory response. Furthermore, S100β staining marked melanoma tumor cells, and diffuse PD-L1 and frequent Ki67-positive staining specifically seen in tumor lesions indicated that the metastatic melanoma cells are immunosuppressive and actively proliferative within the brain (Fig. 5 *F*–*K*). These data suggest that the syngeneic mouse model of melanoma brain metastasis is an ideal platform for studying the interaction between tumor cells and the tumor microenvironment, especially the immune system.

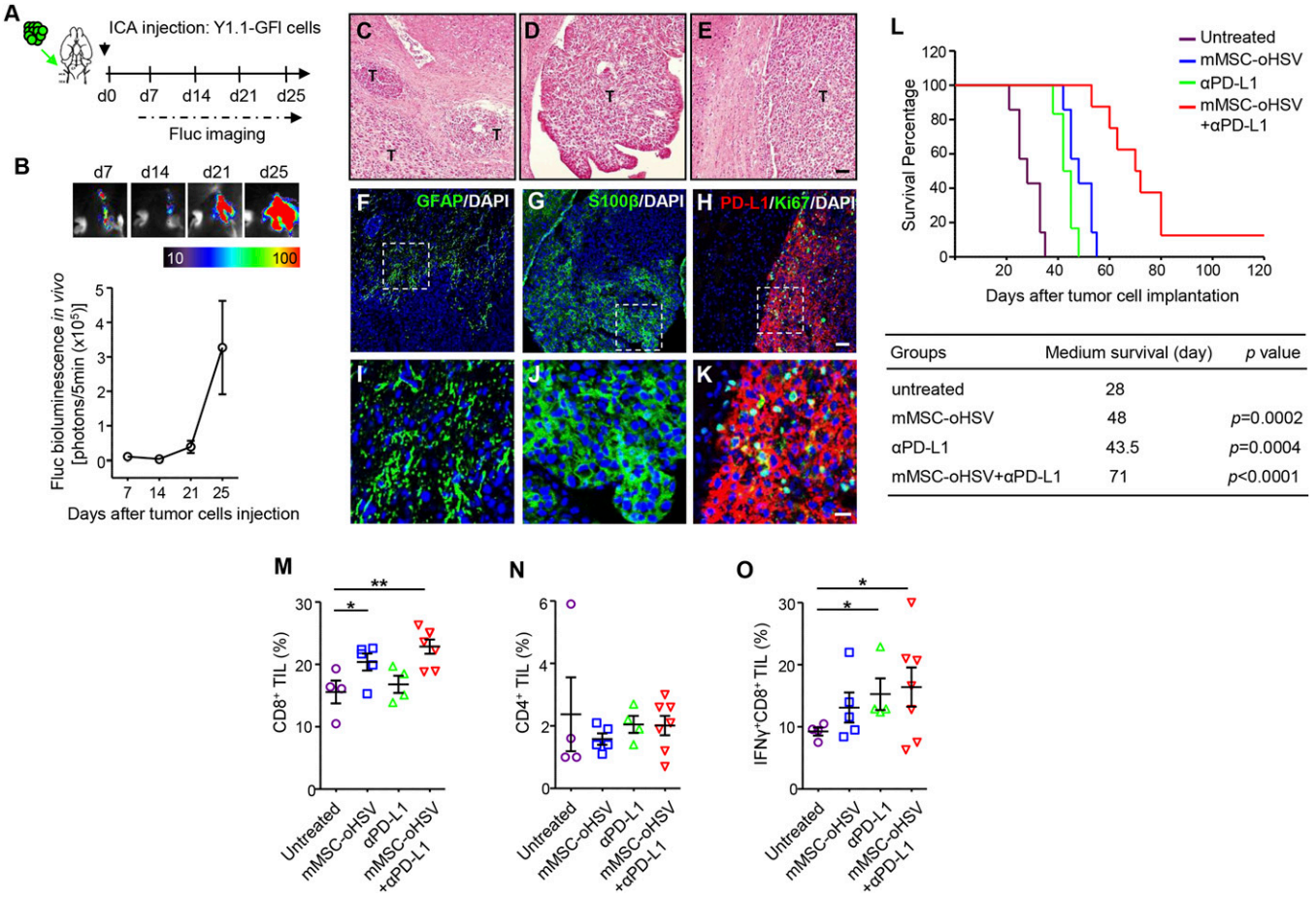


| Groups | Medium survival (day) | *p* value |
|---|---|---|
| untreated | 28 | |
| mMSC-oHSV | 48 | *p*=0.0002 |
| αPD-L1 | 43.5 | *p*=0.0004 |
| mMSC-oHSV+αPD-L1 | 71 | *p*<0.0001 |

**Fig. 5.** Combined therapeutic efficacy of mouse MSC-oHSV and αPD-L1 in a syngeneic mouse model of melanoma brain metastasis. (*A*) Experimental outline. Green arrow indicates the route of tumor cell injection. Black arrow indicates the time point for tumor implantation. (*B*, *Top*) Representative bioluminescent images showing mice ICA-injected with Y1.1-GFl cells. (*B*, *Bottom*) Plot showing the in vivo bioluminescence intensity of metastatic tumor growth in the syngeneic mouse model ($n$ = 5 mice). (*C*–*E*) H&E histology images showing multiple metastatic foci present in the brains of mice bearing melanoma brain metastases. T, tumor area. (Scale bar: 50 μm.) (*F*–*K*) Immunofluorescence analysis of mouse GFAP, S100β, PD-L1, and Ki67 in adjacent brain sections of mice bearing melanoma brain metastases (Scale bars: 50 μm in *F*–*H*, 20 μm in *I*–*K*). Nuclei were stained with DAPI. (*L*) Kaplan–Meier survival curves of melanoma brain metastasis-bearing mice treated with mMSC-oHSV ($n$ = 7 mice), αPD-L1 ($n$ = 6 mice), mMSC-oHSV + αPD-L1 ($n$ = 8 mice), or untreated ($n$ = 7 mice). The table presents the medium survival for each group and a comparison of the treated and untreated control groups (log-rank test). (*M*–*O*) Proportion of indicated cell populations determined by flow cytometry. Bars indicate mean values and SE. *$P$ < 0.05, **$P$ < 0.01 vs. untreated controls.

**MSC-oHSV and Anti–PD-L1 Have Combined Therapeutic Efficacy in a Syngeneic Melanoma Brain Metastasis Mouse Model.** We next examined the sensitivity of YUMM1.1 cells to oHSV infection in vitro. oHSV infection greatly decreased YUMM1.1 cell viability, which was associated with the production of oHSV over time (*SI Appendix*, Fig. S9 *B* and *C*). Coculture of YUMM1.1 and mouse MSCs freshly loaded with oHSV (mMSC-oHSV) resulted in a significant decrease in YUMM1.1 cell viability (*SI Appendix*, Fig. S9*D*). To test the therapeutic efficacy of mMSC-oHSV in combination with anti–PD-L1 antibody (αPD-L1) administration, mice bearing melanoma brain metastases were divided into four groups: control (untreated), treated with αPD-L1 (i.p. injection), mMSC-oHSV (ICA injection), and mMSC-oHSV + αPD-L1. A significant survival benefit was achieved by both αPD-L1 and mMSC-oHSV monotherapy; however, the combined therapy of mMSC-oHSV + αPD-L1 provided much greater survival extension than either monotherapy (Fig. 5*L*). In parallel, we also tested the efficacy of BRAF inhibitor PLX4720 on the survival of tumor-bearing mice. The results revealed that PLX4720 slightly prolonged mice survival; however, the tumor growth eventually led to mortality (*SI Appendix*, Fig. S10). Flow cytometry analysis of tumor-infiltrating T lymphocytes demonstrated a greatly increased $CD8^+$ fraction in the group of mice treated with mMSC-oHSV + αPD-L1 compared with the untreated control group (Fig. 5*M* and *SI Appendix*, Fig. S11), whereas no significant changes in the $CD4^+$ TIL subset were seen among the four groups (Fig. 5*N*). Within the $CD8^+$ cell population, more IFNγ-producing $CD8^+$ cells were found within the brain of mice treated with mMSC-oHSV + αPD-L1 compared with those of the untreated control group (Fig. 5*O*), suggesting that infiltrating cytotoxic $CD8^+$ TIL may play a role in eradicating metastatic tumor cells in the brain. These results strongly suggest that PD-L1 immune checkpoint blockade significantly improves the therapeutic efficacy of MSC-based oncolytic virotherapy in melanoma brain metastasis.

## Discussion

In this study, we show that oHSV has a potent cell-killing effect in a broad spectrum of malignant melanoma lines. To explore the therapeutic efficacy of oHSV in melanoma brain metastasis, we created in vivo imageable mouse models of melanoma brain metastasis in both immunocompromised and immunocompetent mice. We demonstrate that ICA-delivered MSC-oHSV, but not purified oHSV, efficiently track metastatic tumor deposits in the brain, suppress brain tumor growth, and prolong survival in mouse models of melanoma brain metastasis. Furthermore, our studies demonstrate that the combination therapy of MSC-oHSV and anti–PD-L1 has improved therapeutic efficacy in syngeneic mouse model of melanoma brain metastasis, which is associated with an increased $CD8^+IFN\gamma^+$ TIL population.

Melanomas are molecularly heterogeneous tumors bearing different mutations and are resistant to a number of currently used chemotherapies (25, 26). In this study, we screened a panel of seven melanoma cell lines consisting of both established and patient-derived brain metastatic melanoma lines for their responses to oHSV infection and oncolysis. Our results reveal that oHSV infection has a consistent cell-killing effect on melanoma lines regardless of their BRAF mutational status, thus strongly supporting the use of oHSV for treating melanoma brain metastasis. Our screening results also demonstrated that the yields of oHSV in melanoma lines correlate with the efficiency of oHSV-mediated cell killing, suggesting that virus replication underlies the direct oncolytic effects. We also found that the oHSV yield in the patient-derived brain metastatic melanoma cell line M15 was relatively lower than that in the other melanoma lines, which correlated with less cell death in M15 cells treated with oHSV. Compared with MeWo, M12, and MSCs, M15 melanoma cells have decreased expression of Nectin-1 receptor, a major cell surface receptor for HSV entry (*SI Appendix*, Fig. S12), which may contribute to less permissive entry of oHSV into M15 cells. However, our data show that oHSV achieves better infection and spread in M15 cells at higher MOI (*SI Appendix*, Fig. S13 *A* and *B*). Based on our previous findings that the efficacy of oHSV-mediated cell killing can be significantly increased using a proapoptotic variant of oHSV, oHSV-TRAIL, in tumor lines that are less permissive to oHSV-mediated oncolysis (27), our future studies will focus on testing the efficacy of oHSV-TRAIL in such melanoma lines.

To test the therapeutic effects of oHSV in melanoma brain metastasis, we developed and extensively characterized in vivo imageable mouse models of melanoma brain metastasis that display the various features of brain metastasis observed in patients with advanced melanoma. Melanoma brain metastasis originates either directly from primary melanoma lesions or from metastatic lymph nodes and visceral lesions (13); therefore, we chose MeWo (derived from the metastatic lymph nodes in advanced melanoma) and M12 (derived from melanoma brain metastases) to mimic these two types of metastasis. These two melanoma lines are either *BRAF* WT or mutant ($BRAF^{V600E}$), the most frequent BRAF mutation seen in melanoma patients (28). Our results indicate that ICA injection of such lines results in the formation of clinically relevant mouse models that resemble the diverse features of metastatic melanoma, including widely disseminated numerous foci in the brain, aggressive and fatal growth, different mutational status of *BRAF*, and pigmented and nonpigmented lesions. These mouse models provide a unique and valuable platform for testing existing and novel therapeutic approaches for melanoma brain metastasis and help us better understand the pathogenesis of melanoma brain metastasis.

Previous studies typically used either intratumoral injection of oHSV into solid tumor lesions or systemic injection of high-dose oHSV (19, 29, 30). Given the multiple metastatic melanoma lesions in the brain, intratumoral injection into each single lesion is not a feasible approach. Systemic delivery of high-dose viruses carries a risk of virus-related toxicity (31). ICA delivery of oHSV has been explored previously in multiple glioblastoma and breast cancer brain metastasis models (32, 33); however, its efficiency is largely impeded by either antiviral activity present in plasma or undamaged BBB. Moreover, our studies have shown that ICA injection of purified oHSV ($2 \times 10^6$ pfu) is unable to access multiple metastatic lesions in the brain. To overcome this limitation, we developed a strategy that uses MSCs as cellular carriers to shield oHSV from neutralization and achieve onsite delivery of oHSV to multiple tumor deposits in the brain. Stem cells, such as MSCs, are promising cell carriers for various antitumor viruses mainly because they can home to tumor deposits in the brain (34–37), can be easily isolated from patients and grown in culture, and have high metabolic activity, which is important for virus production (20, 38). Furthermore, MSCs are less immunogenic (39) and have been used in various clinical trials for different indications (40). In addition, MSCs also have been used as virus carriers in a phase 1 clinical trial in ovarian cancer patients (41). Using oHSV mutants bearing diagnostic proteins combined with bioluminescence and fluorescence imaging, our experiments reveal that MSCs act as oHSV carriers and track metastatic tumor deposits in the brain, ultimately releasing the oHSV. Our in vivo imaging data suggest that after ICA injection of MSC-oHSV-Fluc, virus replication initially occurs within infected MSCs, which releases oHSV-Fluc upon cell lysis, transfers oHSV to adjacent tumor cells, and results in subsequent virus replication in tumor cells. Comparison of the accessibilities of MSC-oHSV and purified oHSV to metastatic tumor lesions in the brain reveals that MSC-oHSV has superior tumor-tracking capability and results in a significant reduction in tumor foci and a survival advantage in mice bearing melanoma brain metastases. Importantly, ICA injection of MSC-oHSV was safe, and we did not observe any acute systemic toxicities or local adverse events, such as brain infarction. Although the mechanism of oHSV-mediated killing of MSCs

remains unclear, our results indicate that it is not mediated via apoptosis due to the absence of cleaved PARP, a hallmark of cell apoptosis (*SI Appendix*, Fig. S14).

The CNS is protected by the BBB and the blood-cerebrospinal fluid barrier, which prevent most therapeutic agents from entering into the brain. Although studies have shown increases in BBB permeability in various brain tumor models, it remains the key mitigating factor for delivering therapeutics into the CNS. Given that delivery of therapeutic agents to the tumors in the brain is a major challenge, significant efforts have been made to develop efficient delivery routes to brain tumors, which include both invasive and noninvasive administration strategies (42). In a previous study, we showed that local implantation of encapsulated MSCs loaded with oHSV have therapeutic efficacy in mouse models of resected brain tumors (21). Recent studies have shown that i.v. injected MSC-oHSV have therapeutic efficacy in treating lung metastatic tumors (43). These studies imply that i.v.-injected MSC-oHSV would be more suitable for treating both primary and metastatic tumors in the lungs as opposed to the tumors in the brain. Therefore, exploring alternate routes of administration of MSC-oHSV to tumors in the brain was critical.

Immune checkpoint blockade is a major advance in recent cancer therapy, especially for the treatment of metastatic melanoma (44), which is typically immunogenic, likely due to the large numbers of UV-associated mutations (45). Two monoclonal antibodies that block PD-1/PD-L1 interactions (pembrlizumab and nivolumab) have shown objective responses in 30∼40% of patients with melanoma brain metastasis (46, 47). oHSV represents a novel approach to tumor immunotherapy and is an attractive option based on its ability to preferentially target, infect, and replicate in cancer cells. Furthermore, oHSV viral genomes can be easily attenuated to limit host pathogenicity or engineered to express immune-potentiating genes to enhance the host antitumor immune response (48). Because PD-1 is activated mostly at tumor sites or other areas of active immune response, the side effects of anti–PD-1/PD-L1 therapy tend to be less severe than those associated with anti–CTLA-4 antibodies, which potentially affect all circulating T cells in the body and thus can cause significant, albeit manageable, autoimmune side effects (49). Meanwhile, our results showed strong PD-L1 expression in melanoma brain metastasis in the syngeneic mouse model. We thus chose to use an anti–PD-L1 immune-checkpoint blocker to antagonize the immune suppression posed by metastatic melanoma cells.

Our study investigated the therapeutic efficacy of MSC-oHSV in combination with anti–PD-L1 for melanoma brain metastasis. We found that $CD8^+IFN\gamma^+$ TIL population was associated with the survival benefits achieved by the combination therapy of MSC-oHSV plus anti–PD-L1, suggesting that cytotoxic $CD8^+$ TIL may play a critical role in killing metastatic melanoma cells in the brain, likely via activation of IFNγ-related signaling pathways. Release of IFNγ at the tumor site could limit oHSV spread but trigger a variety of beneficial responses, such as activation of other immune cell subsets, up-regulation of MHC class I, and antiangiogenesis. The transient nature of IFNγ secretion likely would limit the detrimental impacts of IFNγ-induced inflammatory reactions in the brain. The overall cellular responses to the oHSV infection, coupled with the release of tumor antigens by virally infected dying tumor cells into the tumor microenvironment, attract innate and adaptive immune cells, including tumor-specific $CD4^+$ and $CD8^+$ T cells. This oHSV infection-mediated response makes virotherapy an ideal modality to combine with immune checkpoint blockers to achieve a more durable response and outcome. Our data suggest that the increased population of $CD8^+IFN\gamma^+$ TIL represents a beneficial antitumor immune response elicited by MSC-oHSV therapy for melanoma brain metastasis.

In conclusion, we have shown that intra-arterial delivery of MSC-loaded oHSV can effectively track and kill metastatic melanoma cells in the brain, and that combination therapy with an immune checkpoint blocker boosts the therapeutic efficacy of MSC-oHSV. Thus, our study warrants clinical testing of MSC-oHSV alone or in combination with immune checkpoint blockers for patients with melanoma brain metastases. Attributed to their innate tumor tropism, stem cells carrying oHSV have been shown to target tumor lesions in the lung and prevent metastases upon i.v. injection (43). Based on previous findings and our present findings, stem cell-based oncolytic virotherapies could have the potential to be broadly applicable in targeting metastatic lesions in organs such as the liver, colon, and lung.

## Materials and Methods

Detailed information on the materials and methods used in this study is provided in *SI Appendix*. All of the animal studies were approved by Massachusetts General Hospital's institutional review board.

**Cell Lines.** MeWo, SK-Mel-2, SK-Mel-28, MALME-3M, and YUMM1.1 melanoma cells were cultured in DMEM (MeWo, MALME-3M, and YUMM1.1) or RPMI (SK-Mel-2 and SK-Mel-28) supplemented with 10% FBS and 1% penicillin-streptomycin. TXM-13 cells were kindly provided by I. J. Fidler and cultured in TXM medium (MEM supplemented with 10% FBS, 1% vitamin, 1% sodium pyruvate, 1% nonessential amino acid, and 1% penicillin-streptomycin). M12 and M15 patient-derived melanoma brain metastatic lines (kindly provided by J. Sarkaria, Mayo Clinic, Rochester) were cultured in DMEM supplemented with 10% FBS and 1% penicillin-streptomycin. Human and mouse MSCs were cultured in NutriStem XF Medium and MesenCult MSC Basal Medium, respectively. Normal human astrocytes were grown in DMEM supplemented with 10% FBS and 1% penicillin-streptomycin.

**Engineered Viral Vectors, Viral Packaging, and Transduction of Tumor Cells.** The following lentiviral constructs were used in this study: Pico2-Fluc-mCherry and Pico2-Fluc-GFP. Lentiviral packaging was performed by transfection of 293T cells as described previously (50). MeWo and M12 cells were transduced at an MOI of 5 in medium containing protamine sulfate (10 μg/mL). All cells were visualized by fluorescence microscopy for GFP or mCherry expression to confirm transduction. oHSV-mCherry and oHSV-Fluc were previously generated by cloning mCherry or Fluc cDNA under the HSV IE4/5 immediate early promoter or CMV promoter, respectively, using site-specific recombination between the G47delta BAC and the shuttle plasmid (27, 51). All of the recombinant oHSVs express *Escherichia coli* lacZ driven by endogenous ICP6 promoter.

**Statistical Analysis.** Data were analyzed using the Student *t* test when comparing two groups and ANOVA when comparing more than two groups. Data were plotted as mean ± SEM, and differences were considered significant at $P < 0.05$. Survival curves were compared using the log-rank test. Analyses were done using GraphPad Prism 5.01.

**ACKNOWLEDGMENTS.** We thank Mark Schroeder and Jan Sarkaria for providing patient-derived M12 and M15 tumor lines, Yohei Kitamura and Deepak Bhere for helping with the in vivo M12 tumor model, Jennifer Lo for assisting with the melanoma cell culture, and Ravi Mylvaganam for FACS analysis. This work was supported by Department of Defense Idea Award CA140744 (to K.S.) and National Institutes of Health Grants R01 CA204720 (to K.S.), P01 CA163222 (to D.F.).

1. Siegel RL, Miller KD, Jemal A (2016) Cancer statistics, 2016. *CA Cancer J Clin* 66:7–30.
2. Fidler IJ, Schackert G, Zhang RD, Radinsky R, Fujimaki T (1999) The biology of melanoma brain metastasis. *Cancer Metastasis Rev* 18:387–400.
3. Sampson JH, Carter JH, Jr, Friedman AH, Seigler HF (1998) Demographics, prognosis, and therapy in 702 patients with brain metastases from malignant melanoma. *J Neurosurg* 88:11–20.
4. Long GV, et al. (2012) Dabrafenib in patients with Val600Glu or Val600Lys BRAF-mutant melanoma metastatic to the brain (BREAK-MB): A multicentre, open-label, phase 2 trial. *Lancet Oncol* 13:1087–1095.
5. Ramanujam S, Schadendorf D, Long GV (2015) Systemic therapies for melanoma brain metastases: Which drug for whom and when? *Chin Clin Oncol* 4:25.
6. Tas F (2012) Metastatic behavior in melanoma: Timing, pattern, survival, and influencing factors. *J Oncol* 2012:647684.
7. Ramakrishna N, Margolin KA (2013) Multidisciplinary approach to brain metastasis from melanoma: Local therapies for central nervous system metastases. *Am Soc Clin Oncol Educ Book* 2013:399–403.
8. Brown P, et al. (2015) A phase III randomized trial of whole brain radiation therapy (WBRT) in addition to radiosurgery (SRS) in patients with 1 to 3 brain metastases. *J Clin Oncol* 33:15.

9. Bentolila LA, et al. (2016) Imaging of angiotropism/vascular co-option in a murine model of brain melanoma: Implications for melanoma progression along extravascular pathways. *Sci Rep* 6:23834.
10. Zou Z, et al. (2016) Convection-enhanced delivery of sorafenib and suppression of tumor progression in a murine model of brain melanoma through the inhibition of signal transducer and activator of transcription 3. *J Neurosurg* 124:1310–1318.
11. Bahrambeigi V, Ahmadi N, Salehi R, Javanmard SH (2015) Genetically modified murine adipose-derived mesenchymal stem cells producing interleukin-2 favor B16F10 melanoma cell proliferation. *Immunol Invest* 44:216–236.
12. Fonkem E, et al. (2012) Melanoma brain metastasis: Overview of current management and emerging targeted therapies. *Expert Rev Neurother* 12:1207–1215.
13. Fidler IJ (2015) The biology of brain metastasis: Challenges for therapy. *Cancer J* 21: 284–293.
14. Liu TC, Galanis E, Kirn D (2007) Clinical trial results with oncolytic virotherapy: A century of promise, a decade of progress. *Nat Clin Pract Oncol* 4:101–117.
15. Lawler SE, Chiocca EA (2015) Oncolytic virus-mediated immunotherapy: A combinatorial approach for cancer treatment. *J Clin Oncol* 33:2812–2814.
16. MacKie RM, Stewart B, Brown SM (2001) Intralesional injection of herpes simplex virus 1716 in metastatic melanoma. *Lancet* 357:525–526.
17. Andtbacka RH, et al. (2015) Talimogene laherparepvec improves durable response rate in patients with advanced melanoma. *J Clin Oncol* 33:2780–2788.
18. Harrington KJ, et al. (2015) Clinical development of talimogene laherparepvec (T-VEC): A modified herpes simplex virus type-1-derived oncolytic immunotherapy. *Expert Rev Anticancer Ther* 15:1389–1403.
19. Russell SJ, Peng KW, Bell JC (2012) Oncolytic virotherapy. *Nat Biotechnol* 30:658–670.
20. Shah K (2012) Mesenchymal stem cells engineered for cancer therapy. *Adv Drug Deliv Rev* 64:739–748.
21. Duebgen M, et al. (2014) Stem cells loaded with multimechanistic oncolytic herpes simplex virus variants for brain tumor therapy. *J Natl Cancer Inst* 106:dju090.
22. Stuckey DW, Shah K (2014) Stem cell-based therapies for cancer treatment: Separating hope from hype. *Nat Rev Cancer* 14:683–691.
23. Tsao H, Goel V, Wu H, Yang G, Haluska FG (2004) Genetic interaction between NRAS and BRAF mutations and PTEN/MMAC1 inactivation in melanoma. *J Invest Dermatol* 122:337–341.
24. Kaufman HL, Kohlhapp FJ, Zloza A (2015) Oncolytic viruses: A new class of immunotherapy drugs. *Nat Rev Drug Discov* 14:642–662.
25. Tsao H, Chin L, Garraway LA, Fisher DE (2012) Melanoma: From mutations to medicine. *Genes Dev* 26:1131–1155.
26. Lo JA, Fisher DE (2014) The melanoma revolution: From UV carcinogenesis to a new era in therapeutics. *Science* 346:945–949.
27. Tamura K, et al. (2013) Multimechanistic tumor targeted oncolytic virus overcomes resistance in brain tumors. *Mol Ther* 21:68–77.
28. Davies H, et al. (2002) Mutations of the BRAF gene in human cancer. *Nature* 417: 949–954.
29. Varghese S, et al. (2007) Systemic therapy of spontaneous prostate cancer in transgenic mice with oncolytic herpes simplex viruses. *Cancer Res* 67:9371–9379.
30. Kulu Y, et al. (2009) Comparison of intravenous versus intraperitoneal administration of oncolytic herpes simplex virus 1 for peritoneal carcinomatosis in mice. *Cancer Gene Ther* 16:291–297.
31. Ferguson MS, Lemoine NR, Wang Y (2012) Systemic delivery of oncolytic viruses: Hopes and hurdles. *Adv Virol* 2012:805629.
32. Ikeda K, et al. (1999) Oncolytic virus therapy of multiple tumors in the brain requires suppression of innate and elicited antiviral responses. *Nat Med* 5:881–887.
33. Liu R, Martuza RL, Rabkin SD (2005) Intracarotid delivery of oncolytic HSV vector G47Delta to metastatic breast cancer in the brain. *Gene Ther* 12:647–654.
34. Tang Y, et al. (2003) In vivo tracking of neural progenitor cell migration to glioblastomas. *Hum Gene Ther* 14:1247–1254.
35. Aboody KS, et al. (2000) Neural stem cells display extensive tropism for pathology in adult brain: Evidence from intracranial gliomas. *Proc Natl Acad Sci USA* 97: 12846–12851.
36. Shah K, et al. (2005) Glioma therapy and real-time imaging of neural precursor cell migration and tumor regression. *Ann Neurol* 57:34–41.
37. Sasportas LS, et al. (2009) Assessment of therapeutic efficacy and fate of engineered human mesenchymal stem cells for cancer therapy. *Proc Natl Acad Sci USA* 106: 4822–4827.
38. Willmon C, et al. (2009) Cell carriers for oncolytic viruses: Fed Ex for cancer therapy. *Mol Ther* 17:1667–1676.
39. Jacobs SA, Roobrouck VD, Verfaillie CM, Van Gool SW (2013) Immunological characteristics of human mesenchymal stem cells and multipotent adult progenitor cells. *Immunol Cell Biol* 91:32–39.
40. Kim N, Cho SG (2013) Clinical applications of mesenchymal stem cells. *Korean J Intern Med* 28:387–402.
41. Mader EK, et al. (2013) Optimizing patient-derived mesenchymal stem cells as virus carriers for a phase I clinical trial in ovarian cancer. *J Transl Med* 11:20.
42. Laquintana V, et al. (2009) New strategies to deliver anticancer drugs to brain tumors. *Expert Opin Drug Deliv* 6:1017–1032.
43. Leoni V, et al. (2015) Systemic delivery of HER2-retargeted oncolytic-HSV by mesenchymal stromal cells protects from lung and brain metastases. *Oncotarget* 6: 34774–34787.
44. Brahmer JR, et al. (2012) Safety and activity of anti–PD-L1 antibody in patients with advanced cancer. *N Engl J Med* 366:2455–2465.
45. Cancer Genome Atlas Network (2015) Genomic classification of cutaneous melanoma. *Cell* 161:1681–1696.
46. Robert C, et al.; KEYNOTE-006 Investigators (2015) Pembrolizumab versus ipilimumab in advanced melanoma. *N Engl J Med* 372:2521–2532.
47. Wolchok JD, et al. (2013) Nivolumab plus ipilimumab in advanced melanoma. *N Engl J Med* 369:122–133.
48. Cattaneo R, Miest T, Shashkova EV, Barry MA (2008) Reprogrammed viruses as cancer therapeutics: Targeted, armed and shielded. *Nat Rev Microbiol* 6:529–540.
49. Topalian SL, Drake CG, Pardoll DM (2015) Immune checkpoint blockade: A common denominator approach to cancer therapy. *Cancer Cell* 27:450–461.
50. Shah K, et al. (2008) Bimodal viral vectors and in vivo imaging reveal the fate of human neural stem cells in experimental glioma model. *J Neurosci* 28:4406–4413.
51. Cheema TA, et al. (2013) Multifaceted oncolytic virus therapy for glioblastoma in an immunocompetent cancer stem cell model. *Proc Natl Acad Sci USA* 110:12006–12011.